ACS APPLIED MATERIALS & INTERFACES

Letter

www.acsami.org

Au Nanorod Decoration on $NaYF_4$:Yb/Tm Nanoparticles for Enhanced Emission and Wavelength-Dependent Biomolecular Sensing

Palanisamy Kannan,[†] Ferhan Abdul Rahim,[†] Rui Chen,[‡] Xue Teng,[†] Ling Huang,[†] Handong Sun,[‡] and Dong-Hwan Kim*,[†]

[†]School of Chemical and Biomedical Engineering, Nanyang Technological University, 70 Nanyang Drive, Singapore 637457

[‡]Division of Physics and Applied Physics, School of Physical and Mathematical Sciences, Nanyang Technological University, 21 Nanyang Link, Singapore 637371

Supporting Information

ABSTRACT: We introduce gold nanorods (GNRs) decoration on $NaYF_4$:Yb/Tm upconversion nanocrystals (UCNCs) by functionalizing the UCNCs with polyamidoamine generation 1 (PAMAM G1) dendrimer, followed by a single-step seed-mediated growth of long-range GNRs to enhance "biological window" upconversion emission. The up-conversion emission of GNR-decorated UCNCs can be enhanced beyond the level typically obtainable using shell-like structures up to 27-fold enhancement. Also, the enhancement can be tuned at different wavelength regions by varying the GNR aspect ratio. The GNR-decorated UCNC is further modified with 2-thiouracil for nonenzymatic detection of uric acid, revealing a detection limit as 1 pM.

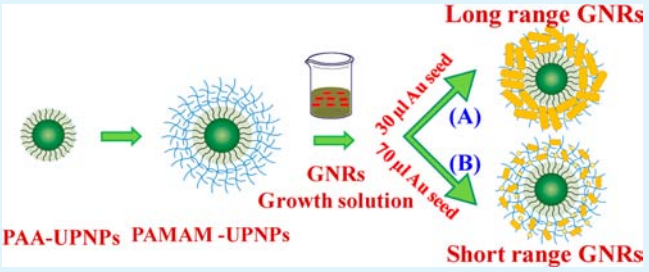

KEYWORDS: *upconversion nanocrystals, gold nanorods, PAMAM, fluorescence enhancements, biosensor*

1. INTRODUCTION

In recent years, lanthanide-based upconversion nanocrystals (UCNCs) have emerged as an efficient and versatile biosensing, bioimaging and therapeutic tool which can overcome inherent limitations of quantum dots and organic dyes, such as photostability, biocompatibility and photoflashing.[1,2] Furthermore, fluorescence emission of UCNCs can be enhanced by placing it in the proximity of a metallic surface;[3−5] metallic nanoshells on UCNCs have shown enhancement factor of several folds up to ~two orders.[6−12] For instance, Xu et al. achieved 14.4 and 12.2-fold emission enhancement at 542 (green) and 656 nm (red region), respectively.[13] Duan et al. selectively enhanced green region emission by 12-fold.[14] Very recently, we have improved 20-fold fluorescence enhancement in violet and green regions by selective growth of metallic nanoshells.[15] Furthermore, enhancement of fluorescence has been difficult to achieve because a continuous metallic shell growth on UCNCs tend to reduce the enhancement efficiency.[16]

In biological applications, fluorescence emission at physiologically relevant wavelengths (700−900 nm) is of particular interest due to the large penetration depth of near-infrared (NIR) light in most biological media. In this regard, gold nanorods (GNR) have been known to possess near- and far-field optical properties which can be precisely tuned throughout the NIR water window by varying their aspect ratio.[17,18] The aspect ratio defines two distinct plasmon resonance frequencies associated with the longitudinal and transverse dimensions of the nanostructure.[19] We therefore hypothesize that GNR, when individually decorated on UCNC surface, represents an excellent candidate for the fluorescent enhancement of UCNCs at selected wavelengths, particularly in the NIR region.

Although several works have reported enhancement of UCNCs using metallic nanospheres,[16,20−22] to the best of our knowledge, the use of an assembly of GNRs to decorate UCNCs have yet to be reported. The aim of this work is to grow two different aspect ratios of GNRs (aspect ratios 1:5 and 1:8) on the UCNCs doped with Er and Tm ions. The transverse and longitudinal SPR bands of GNRs with an aspect ratio of 1:5 were efficiently coupled with fluorescence of Er doped $NaYF_4$:Yb/Er UCNCs at 548 and 657 nm and the enhancement factor was found to be 11.2-fold. On the other hand, the above two SPR bands of GNRs with an aspect ratio of 1:8 were efficiently coupled with fluorescence of Tm doped $NaYF_4$:Yb/Er UCNCs at 470, 550, and 805 nm and the enhancement factor is found to be 27-fold. For the latter case, the longitudinal SPR band is more intense than the transverse band, thus we observed 27-fold enhanced fluorescence of Tm doped UCNCs at selected region ($^3H_4 \rightarrow {}^3H_6$; 805 nm). Furthermore, we enhanced the "biological window" fluorescence peak at 805 nm ($^3H_4 \rightarrow {}^3H_6$) for the first time. The higher-aspect-ratio GNRs have more intense plasmonic proper-

Received: March 1, 2013
Accepted: April 11, 2013
Published: April 11, 2013

 © 2013 American Chemical Society

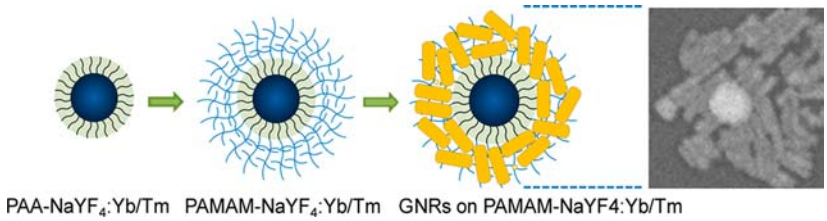

Figure 1. Schematic illustration of the growth of long-range GNRs on PAMAM-functionalized $NaYF_4$:Yb/Tm nanoparticles (UCNCs) and the respective FE-SEM image.

ties and it further improved the fluorescence properties of Tm-doped UCNCs. We have also proven that such use of high aspect ratio GNRs is beneficial, especially for the detection of UA by spectrophotometric method (UV−vis and fluorescence). We have shown with our quantitative data that 27-fold enhancement was obtained using GNR-decorated UCNCs. In contrast to the growth of a continuous nanoshell, which prevents the penetration of fluorescence emission of core UCNC above a certain thickness, we foresee the use of GNR decoration would overcome this limitation because there are gaps between the GNRs. Additionally, unlike zero-dimensional spherical nanoparticles, the use of one-dimensional GNRs offer a higher degree of tunability because the aspect ratio can be precisely controlled.

To prevent the direct adsorption of GNRs on the UCNCs, which would result in fluorescent quenching, we herein employed a layer of polyamidoamine dendrimer generation 1 (PAMAM G1) as a spacer. In contrast to commonly used polyelectrolytes, PAMAM dendrimer represents a more viable option due to two reasons. First, its thickness can be precisely controlled (in this work we use thickness of 2.5 ± 0.1 nm). Because luminescent enhancement of UCNC is dependent on the separation distance between UCNC and metallic nanoparticles,[23] the use of PAMAM would allow for better positional control of our GNRs in order to achieve optimized enhancement. Second, PAMAM itself is an efficient promoter of fluorescence.[24,25] We have observed PAMAM G1-decorated UCNC showing fluorescence enhancement of ∼1.5-fold, indicating fluorescence enhancement property of PAMAM.

Although we mainly focus on the growth of GNRs on $NaYF_4$:Yb/Tm UCNCs, we also performed a comparison with $NaYF_4$:Yb/Er UCNCs to prove our hypothesis that emission enhancement at a different wavelength can be achieved by changing the GNR size. Spherical-shaped $NaYF_4$:Yb/Tm and $NaYF_4$:Yb/Er UCNCs were synthesized by thermal decomposition of rare-earth/sodium trifluoroacetate precursors in the presence of oleic acid (OA) and octadecene (ODE) as reported previously.[26]

2. EXPERIMENTAL SECTION

2.1. Chemicals. YCl_3, $YbCl_3$, $TmCl_3$, $ErCl_3$ (purity >99.9%), trifluoroacetic acid, oleic acid, 1-octadecene, sodium trifluoroacetate, poly(acrylic acid) and polyamidoamine generation 1 (PAMAM G1), $HAuCl_4$, $AgNO_3$, $NH_2OH{\cdot}HCl$, 2-TU, and UA were purchased from Sigma-Aldrich. Cyclohexane, chloroform, and ethanol were supplied by Merck, Singapore. All other chemicals used in this investigation were of analytical grade and were used without further purification.

2.2. Instrumentation and Methods. Field-emission scanning electron microscopy (FE-SEM) was performed on the JEOL instrument (JSM-6700F, Japan) at an acceleration voltage of 5 kV and a working distance between 7 and 8 mm. The crystalline nature and phase purity of the products were examined via XRD using a Bruker AXS D8-advance X-ray diffractometer advanced with Cu Kα radiation (λ = 1.5418 Å), keeping the operating voltage and current at 40 kV and 40 mA, respectively. The 2θ range used was from 0 to 80° in steps of 0.02°, with a count time of 2 s. The photoluminescence (PL) measurements were performed using Horiba Jobin Yvon-FluoroMax-4 at room temperature. A continuous wave diode laser emitting at 980 nm with power 2 W was used as the PL excitation source and the signal was dispersed by a 750 mm monochromator combined with suitable filters and detected by a photomultiplier by using the standard lock-in amplifier technique. All UV spectra were obtained using a UV spectrophotometer (UV-2540, Shimadzu, Kyoto, Japan). The chemical structures of the nanomaterials were analyzed by using Fourier Transform Infrared Spectroscopy (FT-IR, Bruker EQUINOX 55 Duroscope). The resolution of the spectra was 4 cm^{-1} and 100 scans were done. Solution-based ζ-potential measurement was obtained using a ζ-potential analyzer (Nano-ZS Zetasizer with DTS Nano Software, Malvern Instruments, Malvern, UK).

2.3. Synthesis of $NaYF_4$:Yb/Er,Tm Nanoparticles. ***Caution**: It should be noted that the decomposition of the metal trifluoroacetates produces various fluorinated and oxyfluorinated carbon species such as trifluoroacetic anhydride $(CF_3CO)_2O$, trifluoroacetyl fluoride CF_3CF_2COF, carbonyl difluoride COF_2, and tetrafluoroethylene C_2F_4. These species are considered heavily toxic and as such the reaction should be carried out in a well-ventilated hood. Care should also be taken not to inhale any of the evolved gases from the reaction.*

The UCNCs were synthesized by a slight modification of Wang and co-workers method.[26] Typically 1 mmol of $RECl_3$ (RE = Y, Yb, Er, and Tm) was added to a 100 mL flask containing a total amount of 10 mL of 1-octadecene (ODE) and 10 mL of oleic acid (OA). The solution was heated to 160 °C for 30 min under argon and then cooled to room temperature. Subsequently, 10 mL of methanol solution of NH_4F (4 mmol) and NaOH (4 mmol) were added to the flask and the resulting mixture was constantly stirred for 30 min. After removal of methanol by evaporation (70 °C), the solution was then heated to 300 °C under argon atmosphere for 1.5 h and cooled to room temperature. The nanoparticles were precipitated by addition of ethanol, collected by centrifugation process, then washed with 1:4 ratio of cyclohexane and ethanol once, and then 1:1 ratio of water and ethanol for several times (more than four times), and finally redispersed in cyclohexane. Other experimental details and discussions are available in the Supporting Information.

3. RESULTS AND DISCUSSION

FE-SEM images and fluorescence spectra of as-synthesized UCNCs are shown in Figure S1 in the Supporting Information.

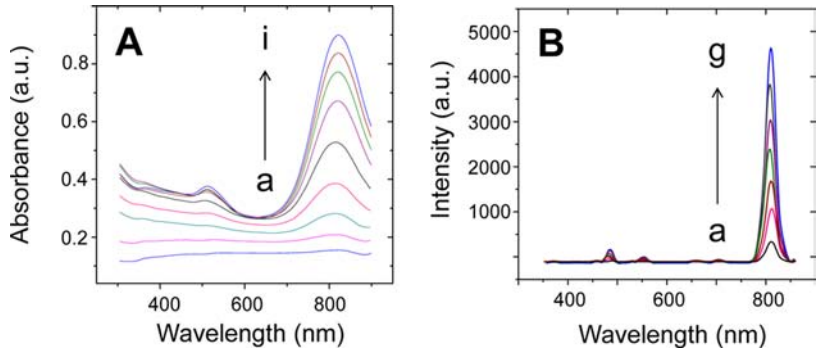

Figure 2. Time-dependent UV−visible absorbance (A) and fluorescence emission (B) spectra of GNRs grown on the $NaYF_4$:Yb/Tm UCNCs. The spectra were recorded at (a−i) 3, 5, 10, 20, 30, 60, 120, 180, and 240 min time intervals and the corresponding emission spectra were recorded at (a−g) 10, 20, 30, 60, 120, 180, and 240 min intervals.

They have relatively smooth surfaces, with an average diameter of about 90 ± 2 nm. From the XRD pattern, we determine that the UCNCs are hexagonal phase mixed with a few cubic impurities (see Figure S2 in the Supporting Information). The as-synthesized UCNCs were then modified to become hydrophilic by ligand exchange method, followed by functionalization with PAMAM G1. The success of this functionalization step was confirmed via FT-IR (see Figure S3 in the Supporting Information).

After the PAMAM modification step, the GNRs were first grown on the surface of $NaYF_4$:Yb/Tm UCNCs via single-step growth by mixing UCNCs with the GNRs growth solution containing Au seeds (30 μL as a nucleation agent), CTAB, Ag and ascorbic acid. The representative schematic of GNR decoration on UCNCs is shown in Figure 1. The same set of experiment was then performed to grow shorter GNRs on $NaYF_4$:Yb/Er UCNCs by adjusting the seed volume (70 μL). High-resolution FE-SEM images are available in the Supporting Information (Figure S4). The length of short and long GNRs on UCNCs is calculated as 45 ± 1.5 and 90 ± 2 nm, respectively. The decahedron is one of the basic multiple-twinned structures, which consists of five tetrahedral crystallites with bare (111) surfaces. Furthermore, the XRD pattern of GNRs surrounded UCNCs showed the Au diffraction feature at 38.20°, which corresponds to the nano Au(111) facet of the face-centered cubic crystal structure. This result further confirmed the formation of GNRs grown on the UCNCs (see Figure S5A in the Supporting Information). Energy-dispersive X-ray (EDX) analysis of the GNRs surrounded on UCNCs reveals the existence of Au, Yb^{3+} and Er^{3+} components (see Figure S5B in the Supporting Information).

We also monitored the growth of GNRs on UCNCs in real-time by UV−vis spectroscopy. The UV−vis spectra taken at different time intervals after the addition of the GNR growth solution to the $NaYF_4$:Yb/Tm UCNC (Figure 2A) clearly reflect the growth of GNRs on UCNCs. Generally, we observed that the longitudinal plasmon band of the GNRs appeared 2−3 min after the start of reaction. A slow continuous red-shift occurred after 30 min. As it has been established that the transverse and longitudinal plasmon bands of GNRs undergo a bathochromic shift with increasing aspect ratio,[27,28] we can infer that the aspect ratio of GNRs growing on the UCNCs increases quickly in the beginning of the reaction and then slowly decreases over time. The band observed at 550 nm is ascribed to the transverse mode of the SPR absorption, while the intense band observed at 750 nm is assigned to the longitudinal mode of SPR absorption. In this context, the appearance of two well-separated absorption bands in Figure 2A confirms that synthesized nanoparticles are anisotropic (i.e., GNRs as shown in Figure S4 in the Supporting Information)

The upconversion emission spectra of UCNCs were collected in aqueous solution (ca.1 wt %) under 980 nm diode laser excitation with a power density of ∼2 W cm^{-2}. It can be seen from Figure 2B, up-conversion photo luminescent major bands were resolved at 470 and 805 nm, which correspond to the $^1G_4 \rightarrow {}^3H_6$, and $^3H_4 \rightarrow {}^3H_6$ transitions of Tm ions, respectively. It is also striking that the NIR photo luminescent (PL) band peak at 805 nm is much more intense than all the other up-conversion photo luminescent bands. The integrated area of this NIR up-conversion PL band is calculated to be about ∼25 times higher than that of all other up-conversion photo luminescent bands, suggesting that radiative deactivation of the up-converted energy predominantly occurs through NIR photo luminescence, which is more favorable for bioimaging. On the other hand, GNRs exhibited two absorption bands, one at a shorter wavelength (transverse plasmon resonance, around 520 nm) and the other at a longer wavelength (longitudinal plasmon resonance) around 805 nm. At this point, the $^3H_4 \rightarrow {}^3H_6$ fluorescence (805 nm) is strongly coupled with the longitudinal GNRs peak (805 nm) as shown by the enhanced up-conversion photo luminescent spectra. The up-conversion photo luminescent spectra of UCNCs before and after growth of GNRs are shown in Figure S1d in the Supporting Information and Figure 2B, respectively (for long-range GNRs on the UCNCs). It is clearly observed that the enhancement of up-conversion photo luminescent properties of up-conversion nanocrystals mainly by wavelength dependent. The emission spectra of the UCNCs during GNR growth shows the fluorescence intensity is increasing significantly with respect to the reaction time. Compared to uncoated UCNCs (see Figure S1d in the Supporting Information), GNRs on $NaYF_4$:Yb/Tm yielded a remarkable 27-fold enhanced emission (Figure 2B) as a result of intense GNR-UCNC spectral coupling at 805 nm. Such huge enhancement factor can be attributed to an increased excitation flux originating from local field enhancements at different spectral positions. The emission enhancement due to GNR decoration is highly wavelength-dependent; the enhancement factors in the GNR-decorated $NaYF_4$:Yb/Tm at 805 nm region is much larger than those in the blue region (i.e., 450 and 475 nm). On the other hand, selective enhancement in a different wavelength region can be achieved by controlling the aspect ratio of the GNRs (aspect

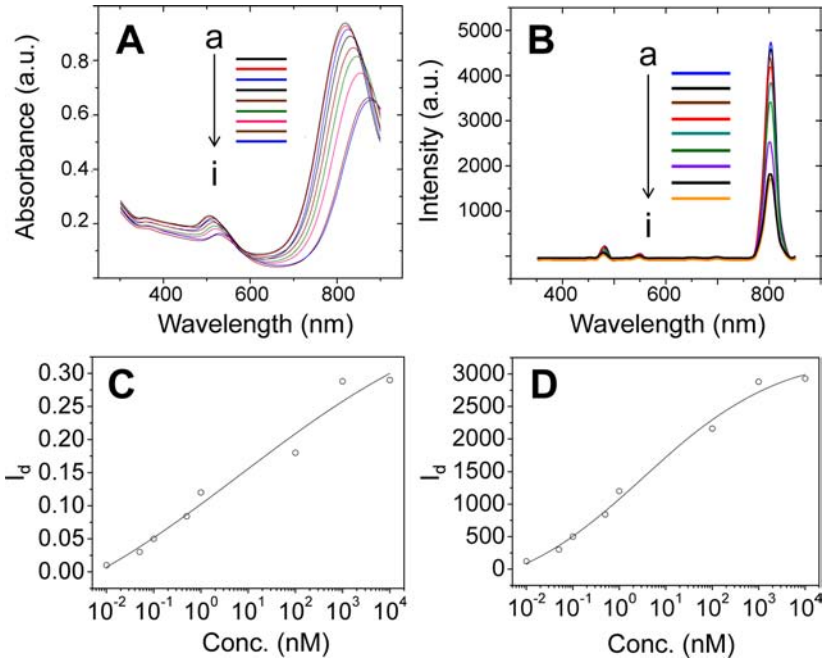

Figure 3. (A) UV−vis and (B) emission spectra of 2-TU functionalized GNRs on $NaYF_4$:Yb/Tm NPs in the presence of variable concentration of UA. (a) 0 nM, (b) 0.01 nM (c) 0.05 nM, (d) 0.1 nM, (e) 0.5 nM, (f) 1 nM, (g) 100 nM, (h) 1 μM, and (i) 10 μM. Figure C and D are the corresponding calibration plot based on UV−vis and emission spectra, respectively.

ratio: 1:5) (see Figure S6 in the Supporting Information). In case of shorter GNRs decorated on $NaYF_4$:Yb/Er, a maximized emission enhancement was achieved at 548 and 657 nm (green and red regions); the enhancement factor was found to be 11.2-fold. The fluorescence intensity of $NaYF_4$:Yb/Tm UCNCs reached saturation after 240 min, implying no further growth of GNRs. This observation clearly demonstrated that the presence of GNRs on up-conversion nanocrystal surface can enhance the up-conversion emission up to the point when GNR growth reaches saturation. In addition, it is interesting to note that the emission enhancement by GNRs is highly wavelength-dependent, as the enhancement factors in the violet/blue, green and red regions are lower than those in the region of 805 nm $^3H_4 \rightarrow {}^3H_6$ fluorescence. Specifically, a 27-fold increase in emission intensity was observed at 805 nm, whereas an increase of only ~6-fold was observed at 470 and 550 nm because of the large coupling distance between long-range GNRs and the corresponding wavelength region.

In this work, we used PAMAM G1 dendrimer as a spacer with a thickness of 2.5 ± 0.1 nm. Prior to the addition of GNRs, we have already tested and optimized the different incubation periods of UCNCs and PAMAM in a reaction mixture to study enhancement arising from PAMAM molecule.[15] Briefly, a solution of 0.5 mM PAMAM-G1 in ethanol was injected into the UCNCs and the mixture was incubated for 1, 2, and 3 h (see Figure S7 in the Supporting Information). The thickness arising from 1, 2, and 3 h incubation of PAMAM G1 on UCNCs was estimated via ellipsometry and found to be 2.2 ± 0.1 nm, 2.5 ± 0.1 nm and 2.6 ± 0.1 nm, respectively. We observed that 1 h incubation of PAMAM G1 on UCNCs can enhance the fluorescence by 1.5-fold compared to unmodified UCNCs, confirming that PAMAM can acts as a fluorescence enhancer. This observation shows that the PAMAM G1 can act as a viable fluorescence enhancer by forming host−guest inclusion complex with UCNPs. Further, the PAMAM G1 dendrimer is 2.5 ± 0.1 nm of length, which is considered as an efficient spacer molecule between gold nanorods and rare-earth up-conversion nanoparticles. We also found that 3 h incubation showed almost the same amount of fluorescence enhancement, i.e., similar to 2 h. Therefore, we chose 2 h as our optimized incubation period providing a thickness of 2.5 ± 0.1 nm.

We then utilized our GNR-decorated $NaYF_4$:Yb/Tm UCNCs for uric acid (UA) detection. UA is an end product of purine nucleotide metabolism in human body. The serum UA level is considered to be a marker of oxidative stress,[29] and the elevated level of serum UA causes several diseases.[30,31] In this work, we employed both plasmonic and fluorescent properties of GNR-decorated UCNCs which would essentially offer sensitive and selective determination of UA. While we used primarily long-range (high aspect ratio) GNR-decorated $NaYF_4$:Yb/Tm UCNCs due to its remarkable fluorescent enhancement factor, moreover same set of experiment was also conducted using short-range GNR-decorated $NaYF_4$:Yb/Er for comparison (see Figure S8 in the Supporting Information).

Upon the addition of UA to 2-thiouracil (TU) functionalized GNR-$NaYF_4$:Yb/Tm, a gradual decrease in absorbance accompanied by a red-shift on the LSPR spectra was observed (Figure 3A). At the same time, fluorescence emission bands appearing at ~805 nm also shows a steady decrease (Figure 3B). At higher concentration of UA (≥10 μM), a 30% decrease in the initial absorbance at LSPR and blue emission peaks of UCNCs were observed. The concurrent and continuous decrease in both LSPR absorption and fluorescence emission intensity clearly indicates that the sensing ability of 2-TU functionalized GNRs toward UA is due to the aggregation of GNRs on UCNCs, which in turn induces spectral changes (aspect ratio 1:8 for Figure 3 and aspect ratio 1:5 for Figure S8 in the Supporting Information). It has been known that the organic moiety, which interacts with metal nanoparticles, alters the electron density of the nanoparticles on the surface, thereby directly affecting the absorbance intensity of the LSPR

dx.doi.org/10.1021/am4007758 | ACS Appl. Mater. Interfaces 2013, 5, 3508−3513

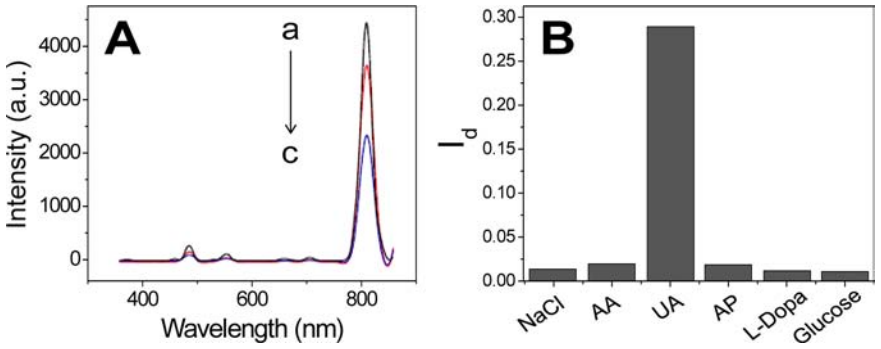

Figure 4. (A) Fluorescence spectra of 2-TU functionalized long-range GNRs on $NaYF_4$:Yb/Tm NPs in the (a) absence and (b, c) presence of blood serum. (b) 1 and (c) 10 μL of serum samples were injected into the nanoparticles. (B) Plot illustrating the selectivity of UA sensing. The change in the emission intensity is plotted against the interfering analytes (1 μM).

band.[32,33] The similar fashion of luminescence drop based sensor was reported for DNA, goat antihuman IgG and gaseous NH_3.[34−36] Further, in both cases, the UCNCs were postfunctionalized with 2-thiouracil (2-TU), which was used as a probe molecule for the capture of UA through hydrogen bonding interactions. The aggregation is instantaneous and it induces spectral change immediately. The FE-SEM measurement evidenced the aggregation of 2-TU functionalized GNRs on UCNCs in the presence of UA (see Figure S9in the Supporting Information). The size of the aggregated nanoparticles is significantly higher than the original nanoparticles. The addition of UA to the unfunctionalized GNRs did not induce any observable change in the spectral response (see Figure S10 in the Supporting Information), indicating no aggregation even at very high concentrations of UA. This suggests that UA could not destabilize unfunctionalized GNRs.

The observed difference in the LSPR absorption/florescence emission intensity upon the addition of UA was plotted against the corresponding concentrations of UA (Figure 3C and D). The calibration plot revealed a linear range of 1 pM to 10 μM. In the plot, I_d refers to the difference in the LSPR absorption/or emission intensity of GNRs in the absence and presence of UA at a given concentration. The detection limit of the this optosensor (GNR-decorated $NaYF_4$:Yb/Tm UCNCs) was experimentally determined to be 1 pM. In comparison, the GNRs-decorated $NaYF_4$:Yb/Er UCNCs managed to achieve a detection limit of 100 nM. Our present detection limit is 3-order higher than a recently reported UA sensor.[37,38] Moreover, our GNR-$NaYF_4$:Yb/Tm-based sensing system showed a high degree of sensitivity in both measurement modes (i.e., LSPR absorption and fluorescence emission). This allows our system to act as a dual-mode sensor offering two measurement options with the same degree of performance. Moreover, this increases the robustness of our system as it does not entirely rely on fluorescence emission. In other words, our system can prospectively be used for dark-field imaging based on LSPR scattering of the GNR-decorated UCNCs. Recently, we reported LSPR scattering studies of GNRs i.e., dark-field studies of GNRs subjected to different polarization angles, and further explored its biosensing capabilities.[39−41] Although the up-conversion fluorescence nanocrystals (UCNCs) are surface plasmon resonance (SPR) inactive, i.e., it does not show any SPR absorption peaks in UV−vis region, the growth of GNRs on the surface of UCNCs will make it SPR active. It has been well-known that the GNRs possess unique transverse and longitudinal plasmonic peaks at ∼520 and 710−1200 nm, of which the peak wavelengths are dependent on the aspect ratio. This also allows us to combine both GNRs and fluoro-active UCNCs as new materials for bioimaging of important model cells by dark-field microscopy.

Finally, we performed UA detection from serum. Figure 4A shows the fluorescence spectral profile of the 2-TU functionalized GNR-$NaYF_4$:Yb/Tm, illustrating good sensing ability in complex media. Significant decreases in the emission intensity at 805 nm were observed during the addition of UA-spiked serum samples (Figure 4A). The recovery of the spiked samples was estimated to be in the range of 96−97%. It should be mentioned here that controlling the pH of the NPs sample is crucial in the optosensing of UA. As the first pKa of UA is 5.8, it cannot have H-bonding interaction with 2-TU functionalized nanoparticles at pH >5.8. Because the pH of our 2-TU functionalized GNRs was 5.2, all measurements were performed with the as-modified UCNCs without any additional procedures to control the pH of the UCNC medium. The selective sensing and quantification of UA is important as other coexisting biomolecules can interfere with the measurement. The selectivity of the assay was examined with the important interfering analytes, including ascorbic acid (AA), acetamidophenol (AP), glucose, L-dopamine (L-DOPA) and sodium chloride (NaCl) at a high concentration of 1 μM (Figure 4B). The presence of excess interferents does not induce any spectral changes the functionalized GNRs on UCNCs, demonstrating the absence of nonspecific aggregation. Despite the interfering analytes (AA, DA, L-dopa and glucose) have H-bonding, they do not interfere with UA detection. For instance, AA could not effectively aggregate the nanoparticles due to the random orientation of TU units around AA anion because AA is not a planar molecule and highly flexible. The interferents have competing H-bonding interactions with water, but UA is hydrophobic. In addition, we believe the selectivity of UA arises from the unique combination of the perfect H-bonding network, possible $\mu-\mu$ and hydrophobic interactions in the same plane (see Figure S11 in the Supporting Information).

4. CONCLUSIONS

In summary, GNRs were individually grown on PAMAM-modified UCNCs for the first time to enhance fluorescence emission efficiency of biological window, beyond the level typically obtainable using shell structures. Under low NIR pumping power density, fluorescent enhancement factor of up to 27-fold in the NIR region were achieved for GNR-decorated $NaYF_4$:Yb/Tm. This suggests that individual GNRs decoration represents a good candidate for the fluorescent enhancement of upconversion nanomaterials. We then demonstrated the

excellent capability of our GNR-modified UCNCs to act as a simple, dual-mode (UV−vis and fluorescence) optical-based UA sensor with high sensitivity and selectivity. The practical utility of the proposed method is verified with real sample analysis.

■ ASSOCIATED CONTENT

Supporting Information

Field emission-scanning electron microscopy (FE-SEM) images, X-ray diffraction pattern of the $NaYF_4$:Yb/Er and $NaYF_4$:Yb/Tm nanocrystals. Procedure for surface modification and growth of GNRs on up-conversion nanoparticles (UCNCs) surface. Time-dependent fluorescence emission of short GNRs grown on $NaYF_4$:Yb/Er. X-ray diffraction pattern of after growth of GNRs on $NaYF_4$:Yb/Er and $NaYF_4$:Yb/Tm nanocrystals. Fluorescence spectra of PAMAM G1incubated into $NaYF_4$:Yb/Tm UCNCs. UV−vis and emission spectra of 2-TU-functionalized GNRs on $NaYF_4$:Yb/Er UCNCs in the presence of variable concentration of UA. UV−vis spectra of unfunctionalized GNRs in the absence and presence of UA. Scheme illustrating of H-bonding interaction between UA and 2-TU functionalized GNRs. This material is available free of charge via the Internet at http://pubs.acs.org.

■ AUTHOR INFORMATION

Corresponding Author

*Tel: (65) 6790-4111. Fax: (65) 6791-1761. E-mail: dhkim@ntu.edu.sg.

Notes

The authors declare no competing financial interest.

■ ACKNOWLEDGMENTS

This work was supported by a research grant from Ministry of Education, Singapore (MOE2012-T2-1-058).

■ REFERENCES

(1) Li, Z.; Zhang, Y.; Jiang, S. *Adv. Mater.* **2008**, *20*, 4765−4769.
(2) Chen, G.; Ohulchanskyy, T. Y.; Kumar, R.; Ågren, H.; Prasad, P. N. *ACS Nano* **2010**, *4*, 3163−3168.
(3) Tam, F.; Goodrich, G. P.; Johnson, B. R.; Halas, N. J. *Nano Lett.* **2007**, *7*, 496−501.
(4) Bardhan, R.; Grady, N. K.; Halas, N. J. *Small* **2008**, *4*, 1716−1722.
(5) Lakowicz, J. R. *Anal. Biochem.* **2001**, *298*, 1−24.
(6) Sudheendra, L.; Ortalan, V.; Dey, S.; Browning, N. D.; Kennedy, I. M. *Chem. Mater.* **2011**, *23*, 2987−2993.
(7) Priyam, A.; Idris, N. M.; Zhang, Y. *J. Mater. Chem.* **2012**, *22*, 960−965.
(8) Xu, W.; Bai, X.; Xu, S.; Zhu, Y.; Xia, L.; Song, H. *RSC Adv.* **2012**, *2*, 2047−2054.
(9) Liu, N.; Qin, W.; Qin, G.; Jiang, T.; Zhao, D. *Chem. Commun.* **2011**, *47*, 7671−7673.
(10) Li, Z.; Wang, L.; Wang, Z.; Liu, X.; Xiong, Y. *J. Phys. Chem. C* **2011**, *115*, 3291−3296.
(11) Wu, Y.; Shen, X.; Dai, S.; Xu, Y.; Chen, F.; Lin, C.; Xu, T.; Nie, Q. *J. Phys. Chem. C* **2011**, *115*, 25040−25045.
(12) Feng, W.; Sun, L.-D.; Yan, C.-H. *Chem. Commun.* **2009**, 4393−4395.
(13) Yuan, P.; Lee, Y. H.; Gnanasammandhan, M. K.; Guan, Z.; Zhang, Y.; Xu, Q.-H. *Nanoscale* **2012**, *4*, 5132−5137.
(14) Zhang, H.; Xu, D.; Huang, Y.; Duan, X. *Chem. Commun.* **2011**, *47*, 979−981.
(15) Kannan, P.; Ferhan, A. R.; Xue, T.; Rui, C.; Sun, H.; Huang, L.; Kim, D. *RSC Adv.* **2013**, DOI: 10.1039/C3RA22130J.
(16) Zhang, H.; Li, Y.; Ivanov, I. A.; Qu, Y.; Huang, Y.; Duan, X. *Angew. Chem., Int. Ed.* **2010**, *49*, 2865−2868.
(17) Guo, L.; Ferhan, A. R.; Lee, K.; Kim, D.-H. *Anal. Chem.* **2011**, *83*, 2605−2612.
(18) Guo, L.; Zhou, X.; Kim, D.-H. *Biosens. Bioelectron.* **2011**, *26*, 2246−2251.
(19) Nikoobakht, B.; El-Sayed, M. A. *Chem. Mater.* **2003**, *15*, 1957−1962.
(20) Rai, V. K.; Menezes, L. d. S.; de Araujo, C. B.; Kassab, L. R. P.; da Silva, D. M.; Kobayashi, R. A. *J. Appl. Phys.* **2008**, *103*, 093526−4.
(21) Schietinger, S.; Aichele, T.; Wang, H.-Q.; Nann, T.; Benson, O. *Nano Lett.* **2009**, *10*, 134−138.
(22) Assumpcao, T. A. A.; da Silva, D. M.; Kassab, L. R. P.; de Araujo, C. B. *J. Appl. Phys.* **2009**, *106*, 063522−4.
(23) Saboktakin, M.; Ye, X.; Oh, S. J.; Hong, S.-H.; Fafarman, A. T.; Chettiar, U. K.; Engheta, N.; Murray, C. B.; Kagan, C. R. *ACS Nano* **2012**, *6*, 8758−8766.
(24) Jasmine, M. J.; Prasad, , E. *J. Phys. Chem. B* **2010**, *114*, 7735−7742.
(25) Stojanovic, N.; Murphy, L. D.; Wagner, B. D. *Sensors* **2010**, *10*, 4053−4070.
(26) Wang, F.; Han, Y.; Lim, C. S.; Lu, Y.; Wang, J.; Xu, J.; Chen, H.; Zhang, C.; Hong, M.; Liu, X. *Nature* **2010**, *463*, 1061−1065.
(27) Pérez-Juste, J.; Liz-Marzán, L. M.; Carnie, S.; Chan, D. Y. C.; Mulvaney, P. *Adv. Funct. Mater.* **2004**, *14*, 571−579.
(28) Sau, T. K.; Murphy, C. J. *Langmuir* **2004**, *20*, 6414−6420.
(29) Becker, B. F. *Free Radical Biol. Med.* **1993**, *14*, 615−631.
(30) Ullman, B.; Wormsted, M. A.; Cohen, M. B.; Martin, D. W. *Proc. Natl. Acad. Sci. U.S.A.* **1982**, *79*, 5127−5131.
(31) Baker, J. F.; Krishnan, E.; Chen, L.; Schumacher, H. R. *Am. J. Med.* **2005**, *118*, 816−826.
(32) Mirkin, C. A. L.; R., L.; Mucic, R. C.; Storhoff, J. J. *Nature* **1996**, *382*, 607−609.
(33) Linnert, T.; Mulvaney, P.; Henglein, A. *J. Phys. Chem.* **1993**, *97*, 679−682.
(34) Wang, M.; Hou, W.; Mi, C.-C.; Wang, W.-X.; Xu, Z.-R.; Teng, H.-H.; Mao, C.-B.; Xu, S.-K. *Anal. Chem.* **2009**, *81*, 8783−8789.
(35) Mader, H. S.; Wolfbeis, O. S. *Anal. Chem.* **2010**, *82*, 5002−5004.
(36) Chen, Z.; Chen, H.; Hu, H.; Yu, M.; Li, F.; Zhang, Q.; Zhou, Z.; Yi, T.; Huang, C. *J. Am. Chem. Soc.* **2008**, *130*, 3023−3029.
(37) Zhang, T.; Sun, X.; Liu, B. *Spectrochim. Acta A* **2011**, *79*, 1566−1572.
(38) Huang, X.; Lan, T.; Zhang, B.; Ren, J. *Analyst* **2012**, *137*, 3659−3666.
(39) Guo, L.; Kim, D.-H. *Chem. Commun.* **2011**, *47*, 7125−7127.
(40) Guo, L.; Huang, Y.; Kikutani, Y.; Tanaka, Y.; Kitamori, T.; Kim, D.-H. *Lab Chip* **2011**, *11*, 3299−3304.
(41) Huang, Y.; Kim, D.-H. *Nanoscale* **2011**, *3*, 3228−3232.